HTML ABSTRACT + LINKS

Ultrafast Charge Dynamics Initiated by High-Intensity, Ultrashort Laser-Matter Interaction

Marco Borghesi*, Lorenzo Romagnani*, Satyabrata Kar*, Toma Toncian[§], Patrizio Antici[†], Patrick Audebert[†], Erik Brambrink[†], Francesco Ceccherini[¶], Carlo A. Cecchetti*, Julien Fuchs[†], Marco Galimberti[#], Leonida A.Gizzi[#], Thomas Grismayer[^], Ralph Jung[§], Andrea Macchi[¶], Patrick Mora[^], Jens Osterholtz[§], Angelo Schiavi[$], Oswald Willi[§]

** School of Mathematics and Physics, The Queen's University of Belfast, Belfast BT7 1NN ,UK*
[§] Heinrich Heine Universität Düsseldorf, Universitätstrasse 1, D-40225 Düsseldorf, Germany
[†] Laboratoire pour l'Utilisation des Lasers Intenses, UMR 7605 CNRS-CEA-Ecole Polytechnique-Univ. Paris VI, 91128 Palaiseau, France
[¶],Istituto Nazionale per la Fisica della Materia (INFM), Dipartimento di Fisica "E. Fermi", Universita' di Pisa, Pisa, Italy
[#],Istituto per i Processi Chimico Fisici-Consiglio Nazionale delle Ricerche, Pisa, Italy
[^] Centre de Physique Theorique, UMR 7644, CNRS-E cole Polytechnique, 91128 Palaiseau, France
[$]Dipartimento di Energetica, Universita' di Roma 1 "La Sapienza", Roma, Italy

Abstract. The interaction of high-intensity laser pulses with matter releases instantaneously ultra-large currents of highly energetic electrons, leading to the generation of highly-transient, large-amplitude electric and magnetic fields. We report results of recent experiment in which such charge dynamics have been studied by using proton probing techniques able to provide maps of the electrostatic fields with high spatial and temporal resolution. The dynamics of ponderomotive channelling in underdense plasmas have been studied in this way, as also the processes of Debye sheath formation and MeV ion front expansion at the rear of laser-irradiated thin metallic foils. An application employing laser-driven impulsive fields for energy-selective ion beam focusing is also presented

Keywords: High-intensity laser-matter interaction, hot electron dynamics, ion acceleration, ion focusing, proton probing.
PACS: 52.38.-r, 52.38.Kd, 52.38.Hb

INTRODUCTION

The interaction of high-intensity laser pulses with matter releases instantaneously ultra-large currents of highly energetic electrons, leading to the generation of highly-transient, large-amplitude electric and magnetic fields. These fields play a role of fundamental importance in many laser-plasma processes. This is particularly true in interactions employing short, ultraintense laser pulses, where enormous currents of very energetic electrons (up to 100-1000 MA) are istantaneously driven via several laser-electron coupling processes. Ultra-large, quasi-static magnetic and electric fields can be generated either by the current flow or via the induced space-charge separation.

CP827, *Superstrong Fields in Plasmas: Third International Conference on Superstrong Fields in Plasmas*, edited by D. Batani and M. Lontano
© 2006 American Institute of Physics 0-7354-0319-8/06/$23.00

Downloaded 27 Aug 2012 to 146.48.102.127. Redistribution subject to AIP license or copyright; see http://proceedings.aip.org/about/rights_permissions

Magnetic fields as large as 10^4-10^5 T and electric fields as large as 10^{12} V/m can be reached in solid target interactions with the laser intensities presently available (up to a few times 10^{20} W/cm^2). Electric fields due to charge separation can drive the expansion of the ions of the plasmas, leading to production of ion beams in interaction with thin foils [1,2], or to Coulomb explosion of plasma channels in interaction with underdense plasmas [3,4]. A major step forward in the detection of such fields has been marked by the development of the proton imaging and deflectometry techniques [5,6], which, employing laser-driven protons as a particle probe, have proven to be an exceptionally useful tool for the investigation of ultrafast plasma dynamics. In this paper, after a brief discussion of the principles of the technique, we will present results from some recent experiments in which proton probes have been used to investigate charge dynamics initiated by the interaction, and the ensuing electric and magnetic fields. An application of transient, laser-initiated fields for control of the angular and spectral properties of a proton beams will be also presented.

PROTON PROBING TECHNIQUES

The unique properties of protons from high intensity laser-matter interactions, particularly in terms of spatial quality and temporal duration, have opened up a totally new area of application of proton probing/ proton radiography. Several experiments have been carried out in which laser-driven proton beams have been employed as a backlighter for static and dynamic target assemblies, in some cases a secondary target irradiated by a separate laser pulse. The proton beams emitted from a laser-irradiated foil are highly laminar [7] and, for projection purposes, can be described as emitted from a virtual, point-like source located in front of the target [8]. A point-projection imaging scheme is therefore automatically achieved. The magnification of the system is determined by $M = 1+L/h$, with L and h respectively the object-to-detector and source-to-object distances. Density variations in the target probed can be detected via modifications of the proton beam density cross section, caused by differential stopping of the ions in the case of thick targets, or by scattering in the case of thin targets. Similarly, electric or magnetic fields in the sampled region can be revealed via the proton deflection and the associated modifications in the proton density pattern.

Probably the most important applications to date of proton probing are related to the unique capability of this technique to detect electrostatic fields in plasmas . This has made possible obtaining for the first time direct information on electric fields arising through a number of laser-plasma interaction processes [9,10,11]. The high temporal resolution, related to the ~ps duration of the proton burst at the source, is here fundamental in allowing the detection of highly transient fields following short pulse interaction.

When the protons cross a region with a non-zero electric field they are deflected by the transverse component $E_\perp$ of the field. The proton transverse deflection at the proton detector plane is equal to

Downloaded 27 Aug 2012 to 146.48.102.127. Redistribution subject to AIP license or copyright; see http://proceedings.aip.org/about/rights_permissions

$$\Delta \mathbf{r}_{\perp} \approx eL \int_0^b \left(\mathbf{E}_{\perp} / m_p v_p^2 \right) dl \qquad (1)$$

where $m_p v_p^2/2$ is the proton kinetic energy, e its charge , b the distance over which the field is present, and L the distance from the object to the detector. As a consequence of the deflections the proton beam cross-section profile undergoes variations showing local modulations in the proton density. Assuming the proton density modulation to be small, i.e. $\delta n/n_0 << 1$, where n_0 and δn are respectively the unperturbed proton density and proton density modulation at the detector plane, we obtain $\delta n / n_0 \approx -\left| div(\Delta \mathbf{r}_{\perp}) \right| / M$ where M is the geometrical magnification. The value of the electric field amplitude and spatial scale can then be determined if a given functional dependence of can be inferred a priori, e.g. from theoretical or geometrical considerations.

Thin meshes inserted in the beam (e.g. between the proton source and the object) are sometimes used as "markers" of the different parts of the proton beam cross sections, in a proper proton deflectometry arrangement [2]. As mentioned earlier, the meshes impress a modulation pattern in the beam before propagating through the electric field configuration to be probed. The beam is so effectively divided in a series of beamlets, and their deflection can be obtained directly from the deflection of the impressed pattern.

A typical set-up for proton probing of high-intensity interaction is shown in fig.1. A high-intensity laser pulse is used to accelerate a beam of MeV protons from the rear surface of a thin metal foils, and this beam is used as a transverse particle probe of the interaction of a second short pulse with a separate target.

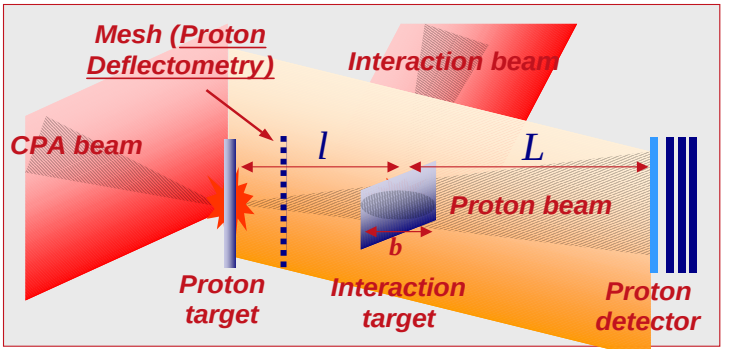

FIGURE 1. Set-up for experiments employing proton probing aimed to the measurement of transient fields.

A general analysis method, applicable to both proton imaging and proton deflectometry data, consists of using particle tracing codes to follow the propagation of the protons through a given three-dimensional field structure, which can be

Downloaded 27 Aug 2012 to 146.48.102.127. Redistribution subject to AIP license or copyright; see http://proceedings.aip.org/about/rights_permissions

modified iteratively until the computational proton profile reproduces the experimental ones. State-of-the-art tracers allow realistic simulations including experimental proton spectrum and emission geometry, as well as detector response

SPACE-CHARGE FIELDS IN UNDERDENSE PLASMAS

The study of the propagation of an intense laser pulse through under-dense plasmas is relevant to a wide range of applications, including laser driven electron acceleration and the fast ignitor scheme for inertial confinement fusion. These application areas demand a detailed study of mechanisms such as laser channelling, self-focusing and the dynamics of the plasma channels caused by Coulomb explosion.

We have recently investigated the interaction of a high intensity ($> 10^{18}$ W/cm^2) laser with an underdense plasma in a recent experimental campaign at the Rutherford Appleton laboratory, by employing the diagnostic technique described in the previous section. The experiment was carried out at the Rutherford Appleton Laboratory, employing the 100 TW Nd-GlassVulcan laser operating in the Chirp Pulse Amplification mode. The dual CPA configuration was employed, providing two CPA pulses with adjustable relative delays at ps precision. Each of the output beams delivered approximately 50 J in 1.2 ps (FWHM) duration. By using off-axis parabolas, the beams were focused down, on different targets, to spots of 10 μm FWHM, with peak intensity reaching about 1.5 10^{19} W/cm^2. One of the beams interacted with the He gas from a supersonic nozzle driven at 50 bar pressure.. The other CPA beam was employed to generate the probe proton beams by irradiating it onto a foil (a 10 μm thick Au foil was typically used). Proton beams were observed having a quasi-Maxwell Boltzmann energy spectrum with temperature and cut-off energy of 3 MeV and 18 MeV respectively. The detector was a multilayered Radio-chromic film (RCF) detector, placed at a distance of 2-3 cms from the gas jet. In the condition of the experiment, this provided a multi-frame temporal scan of the interaction for up to 50 ps in a single shot [1]. The temporal resolution of each frame was typically of the order of few picoseconds, predominantly depending upon the transit time of the protons through the interaction region. The time of arrival of the protons of a given energy at the interaction point was controlled by the relative time of arrival of the split CPA beams on their respective destination. The point projection magnification was approximately 11.

The interaction of the high intensity short pulse laser with the under-dense plasma was observed for a few hundreds of picoseconds, starting from the time of entry of the laser into the field of view of the proton beams. We shall concentrate here on the early stage of the interaction of the laser (of two different intensities) with He gas at 50 bar pressure. The entry of the short pulse into the field of view and its propagation through the plasma were observed due to the generation of an instantaneous electron depleted ion channel under the action of the strong radial ponderomotive force of the laser. The

Downloaded 27 Aug 2012 to 146.48.102.127. Redistribution subject to AIP license or copyright; see http://proceedings.aip.org/about/rights_permissions

positively charged ion channel deflected the probe protons outward from the laser axis along the radial direction, creating a 'negative' shadow of the channel over the RCF. Fig. 2 shows the proton images obtained at two early times of interaction, for two different laser intensities. The proton images of the ion channel show three different characteristic features at different regions, corresponding to different stages of the interaction. They are: (1) a 'bullet' shaped channel (left end of frames (a) and (c)), (2) a 'white' channel (corresponding to lower probe proton flux than the background) with sharp black boundary (all frames), and (3) a white channel with a dark line on axis (left end of frames (b) and (d)).

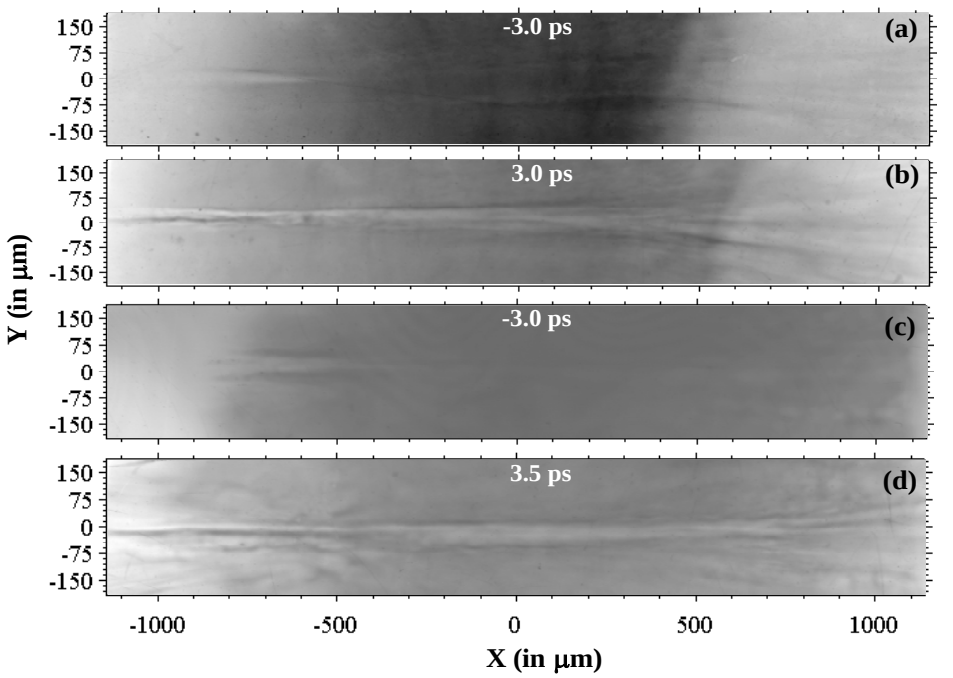

FIGURE 2. Proton projection images showing the different stages of the interaction of a laser pulse propagating through a 50 bar He gas jet. The peak vacuum intensity is 4 10^{18} W/cm^2 (frames (a) and (b)) and 1.5 10^{19} W/cm^2 (frames (c) and (d)).

The images are snapshots of the plasma during the propagation of the laser pulse through the underdense He plasma (the laser prepulse preionizes the gas in the region under observation, as inferred from simultaneous interferometric measurements). The features mentioned above are imprinted in the proton probe cross section due to the effect of the radial fields surrounding the propagation axis at various stages of the plasma evolution during or immediately after the pulse propagation. As the pulse propagates the radial ponderomotive force will expel electrons from the focal region, leaving the inner part of the channel positive charged and setting up a charge-separation electric field. This field will eventually lead to the radial expansion of the channel. However, in the early stages of the interaction one can roughly consider the

Downloaded 27 Aug 2012 to 146.48.102.127. Redistribution subject to AIP license or copyright; see http://proceedings.aip.org/about/rights_permissions

space-charge force acting on the electron in balance with the ponderomotive force. If one assumes that the laser pulse has a spatially and temporally gaussian profile, the radial field at the rising edge of the pulse will cause the pointed bullet-like feature to appear. Close to the peak of the pulse, the strong radial field causes a strong deflection of the probe protons away from the interaction axis, resulting in the "white" channel with dark edges (accumulation regions of the deflected protons). Behind the tail of the pulse, the ponderomotive force is not active anymore and the electrons are attracted back toward the center of the axis. However, at this stage the ions have started to move outwards, away from the axis. In this way, the radial ion density will be depleted on the axis of the channel and therefore will form a finite width 'wall' at some radial position as a function of time. Due to the high temperature of the electrons, gained by the laser ponderomotive force, they will not be efficient to shield completely the ion 'wall'. Inside the wall, towards the axis, their excess charge density may generate a negative electric field which can be seen as the reason of the formation of the central black line along the axis of the channel. This interpretation has been supported by Particle in Cell and Particle Tracing simulations which have qualitatively reproduced the features observed, but will not discuss here in detail due to lack of space.

DEBYE SHEATH FORMATION AND ION EXPANSION ON LASER-IRRADIATED SOLID TARGETS

The acceleration of multi-MeV ion beams following the interaction of short ($t \leq 1$ ps) and intense ($I > 10^{18}$ W/cm^2) laser pulses with thin solid foils has been one of the most active areas of research in the high field science in the last few years. A number of mechanisms have been proposed to explain the acceleration of high energetic ions from laser-irradiated foils. The most relevant mechanism to currently achievable experimental conditions is the so-called Target Normal Sheath Acceleration (TNSA) [12,13,14]. During the interaction with the front surface plasma, the laser pulse transfers its energy, via a number of processes, to a population of fast electrons. The fast electrons propagate to the rear surface of the target, where they form a dense electron plasma sheath. The electric field associated with the plasma sheath, which can be of the order of a few TW/m, ionizes the back of the target and accelerates the ions normal to the target surface. After this initial phase the acceleration proceeds as a plasma expansion into a vacuum, with a well defined expanding ion front. At this stage the accelerating electric field peaks at the ion front, due to the co-moving plasma sheath. As the beam expands the initially fast electrons progressively transfer their energy to the ions and the field decreases until the acceleration eventually ceases.

By employing the proton probing techniques discussed previously, we carried out an experiment in order to investigate the electric fields associated with Debye sheath formation and ion front expansion via the TNSA mechanism. The experiment was performed employing the LULI 100 TW system operating in the Chirped Pulse Amplification mode (CPA). Two laser pulses (CPA_1 and CPA_2) were focused onto two separate targets leading to the acceleration of a proton beam from each target. CPA_1 was focused onto 10 to 40 μm thick aluminium and gold foils (interaction target) at an intensity of ~ 3.5 10^{18} W/cm2. CPA_2 was focused onto a ~10 μm thick gold foil (proton target) at an intensity of ~2 10^{19} W/cm^2. The proton beam from the

Downloaded 27 Aug 2012 to 146.48.102.127. Redistribution subject to AIP license or copyright; see http://proceedings.aip.org/about/rights_permissions

proton target was employed as a transverse charged particle probe for the accelerating electric fields at the back of the interaction target. The interaction targets were bent in order to minimize the effect of global target charge-up observed in previous experiments, which would have prevented from probing close to the target surface. The time delay between CPA_1 and CPA_2, and therefore the proton probing time, could be optically adjusted with ps precision. The proton beams from the two targets were detected employing stacks of several layers of Radiochromic films (RCFs).

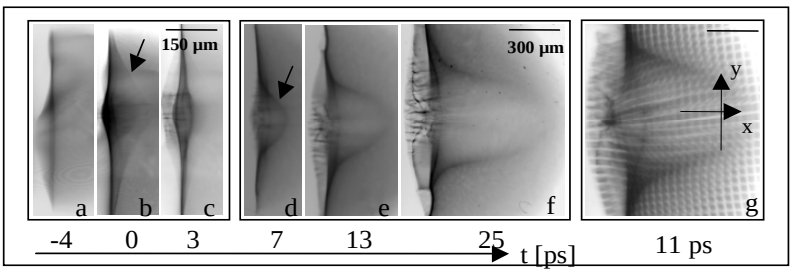

FIGURE 3. (a-f) Proton projection images and (g) Deflectograms of the rear of a bent foil irradiated at the front by an high-intensity laser pulse. Time delays of the snapshots relative to the peak of the interaction pulses are indicated below the frames.

Two qualitatively different structures are observed in Proton Imaging data [15]. Around the peak of the interaction of CPA_1 with the interaction target a transient (t = 0), pronounced deflection of the probe protons is observed (Fig. 3c, indicated by the arrow). The deflection vanishes after a few ps, as can be seen by comparing Fig. 3c-d, and can be attributed to the predicted strong electric field associated with the initial dense and hot electron sheath. The experimentally measured final velocity of the expanding front (Fig. 3a-f) is 3-4 $\times 10^7$ m/s, which is consistent with the detected high energy spectral cut-off of ~ 6-7 MeV of the proton beam emitted from the interaction target. Fig.4 shows the evolution of front position and velocity with time. From the graph, it is seen that the front gains about 70 % of the final velocity in the first 2 ps after the interaction, while only 30 % of the final velocity is acquired at later times, indicating that the proton beam must gain most of its final energy during the initial phase of the acceleration process. It can be noticed form the plots of fig.4 that the overall shape of the experimental curve closely resembles the behavior predicted by theoretical models, with the slope of the curve increasing in the first few ps and then saturating to the final front velocity value.

More quantitative information on the electric field driving the late times acceleration of proton beam was provided by Proton Deflectometry data. The deflection pattern observed in the proton deflectograms (Fig. 3g) reveals an electric field which peaks at the expanding front and is uniform and substantially smaller behind it, in agreement with theoretical predictions.

Downloaded 27 Aug 2012 to 146.48.102.127. Redistribution subject to AIP license or copyright; see http://proceedings.aip.org/about/rights_permissions

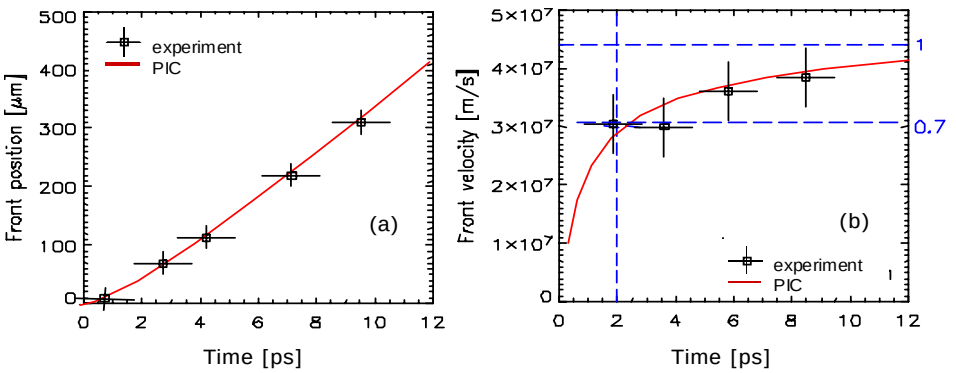

FIGURE 4. (a). Front position along the propagation axis as a function of time. (b) Velocity of the front as a function of time. Both experimental results from a typical shot and 1D PIC simulation simulation results are plotted.

The time and spatially integrated electric field value can be estimated by measuring the mesh line shift in the deflectograms. Referring to Fig. 3g the peak electric field at the expanding front can be estimated to be of the order 10^9 V/m.

The experimental results were also compared with 1-D fluid and Particle In Cell (PIC) simulations of the expansion of an electron-ion plasma of limited width into a vacuum. The initial electron sheath field and the peaked structure of the field at the ion front were observed in the simulations, with a peak field intensity in good agreement with the experimental findings. Excellent agreement with the experiment was also found regarding the evolution in time of the expanding front position and velocity, as shown in fig.4, where typical experimental results and PIC results are compared. The initial conditions for the simulation were estimated on the basis of the experimental parameters, i.e. the electron temperature Te~ 500 keV was chosen from scaling laws for the ponderomotive energy associated to the laser field [13]. Assuming a conversion efficiency into hot electrons of the order of 10% and a divergence of the electrons inside the target of 20º (half-angle), as inferred from measurements available in the literature [16], the electron density at the rear surface was estimated as ~ 3 10^{19} cm^3 on the basis of conservation of energy flux considerations.

A detailed understanding of the accelerating field structure was obtained by comparison of the experimental results with numerical simulations of the propagation of a probe proton beam through a given time-dependent electric field structure. Both Proton Imaging and Proton Deflectometry data, and both the initial transient deflection and the expanding front at later times, were simulated. The broad spectral content of the probe proton beam was taken into account. Field patterns with cylindrical symmetry were assumed, as it was verified that the bent geometry of the target has negligible effect.

In the case of the transient initial deflection the field was assumed normal to the target surface, and the dependence of the field on z (coordinate along the symmetry axis) and time was chosen in order to mimic the profiles suggested by the 1D PIC simulations. A gaussian dependence of the field on the radial coordinate ρ was chosen. As shown in fig.6 (a), the simulation reproduced well the data (compare with fig. 3

Downloaded 27 Aug 2012 to 146.48.102.127. Redistribution subject to AIP license or copyright; see http://proceedings.aip.org/about/rights_permissions

(b)), provided that an artificial truncation of the field profile was introduced at a distance h from the target (with best match obtained for h~ 20 μm). This suggests a finite extension of the electron cloud, perhaps corresponding to the maximum excursion from the target of the trapped electrons (i.e. the electrons which are not energetic enough to reach infinity). The problem of the finite extension of the electron cloud, leading to a finite extension of the electric field has been discussed in [17].

The simulations of front expansion at later times confirmed that an electric field with the expected peaked structure is required in order to reproduce the experimentally observed probe proton deflection (Fig. 5c), with a peak field value in reasonable agreement with PIC and fluid predictions. The best match with the experiment at t=11 ps (case of fig.2(g)) was found for a field of $2.5\ 10^9$ V/m at peak and of 10^8 V/m in the plateau region.

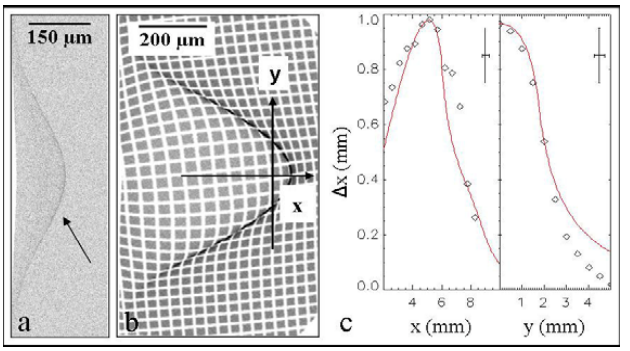

FIGURE 5. (a,b) Particle tracing simulations of experimental data in Fig. 3b and Fig 3g. (c) Comparison of the deflection in the x direction measured along the x and y axes in the experiment (scatter graph) and in the particle tracing simulations (line).

Circular or elongated zones of probe proton depletion, delimited by narrow lines of high density probe proton accumulation, symmetrically located at the two sides of the expanding proton front have been observed in several shots (see fig.6). These structures appear near the peak of the interaction pulse and last for several tens of ps. Similar structures have also been observed on wire shots at lower intensities. A possible interpretation for these structures is that they relate to toroidal magnetic fields surrounding the base of the expanding ion front. These fields could be due to circulation of electrons which are first expelled from the target in proximity of the interaction axis and then fall back to the target in a fountain-like fashion, as also sketched in fig.6. Particle tracing simulations have shown that the structures are fully compatible with such magnetic field configuration, if we assume that the field lines will bend following the foil surface. This is essential for producing two well separated structures as observed.

Downloaded 27 Aug 2012 to 146.48.102.127. Redistribution subject to AIP license or copyright; see http://proceedings.aip.org/about/rights_permissions

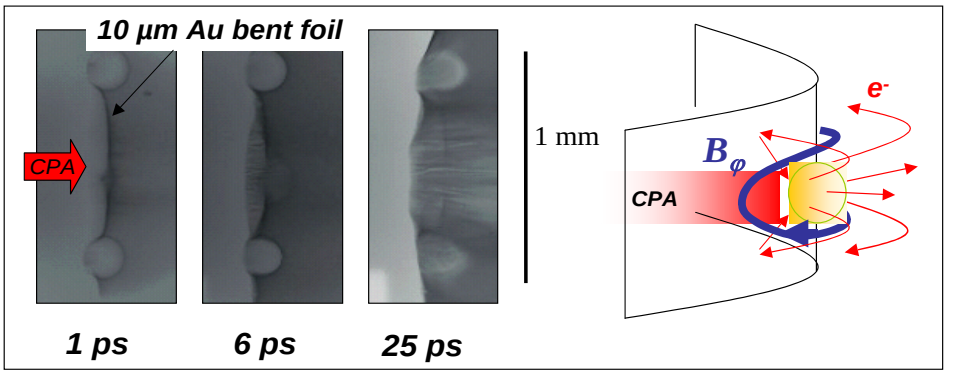

FIGURE 6. Proton projection images showing spherical structures at the rear of bent targets at different observation times relative to the peak of the interaction pulse. A sketch of the possible magnetic field and electron current configuration producing the structure observed is also provided.

Upon exiting from the target rear surface the electrons cannot travel long distances away from the target, because the space-charge field at the target-vacuum interface tends to recall them back. On the other hand in the direction parallel to the target surface the electrons can travel a larger distance, as in this case the charge imbalance can be compensated by the return current provided by cold electrons in the target. The maximum distance they can travel is set by energy conservation if one takes into into account ohmic losses for the cold electrons current inside the target. Simple estimates based on this suggest maximum propagation distances of the order of the mm (i.e. of the same order of magnitude of the distance of the spherical structure from the symmetry axis).

USE OF IMPULSIVE LASER FIELDS FOR PROTON BEAM PROPERTIES CONTROL

The transient electrostatic fields described in the previous section offer novel opportunities as a tool for controlling the properties of proton beams. In particular, while probing ion front expansion from hemi-cylindrical targets, it was seen that not only the ion front accelerated from the hemi-cylinder went through a focus (as expected from ballistic focusing prediction [18] and previous experimental evidence [19])but also that, under certain conditions, the transient fields at the rear of the target caused the protons of the probe beam to form a caustic at the center of the hemi-cylinder. This suggested the idea of using a laser-irradiated hollow cylinder as a tool for varying the angular properties of a proton beam. Indeed the arrangement proved to work effectively as a laser driven micro-lens able to focus controllably laser-accelerated proton beams.

Downloaded 27 Aug 2012 to 146.48.102.127. Redistribution subject to AIP license or copyright; see http://proceedings.aip.org/about/rights_permissions

Its operation was demonstrated in an experiment also carried out at the LULI Laboratory, employing the 100 TW laser operating in the Chirped Pulse Amplification mode (CPA). One of the two pulses (irradiance I=3 10^{19} W/cm^2) was used to accelerate a high-current, diverging beam of up to 15 MeV protons from a 10μm thick Au foil target. The other pulse (I = 3 10^{18} W/cm^2) was focused onto the side of a hollow cylinder. The proton beam from the first foil was directed through the cylinder and detected with a stack of Radiochromic Films, which was shielded with an 11 μm Al foil allowing protons with energies above 1.5 MeV to be recorded. Various experimental parameters including the length, diameter and material of the cylinders were varied to study the focusing characteristics of the proton beam under different conditions. At a source-cylinder distance of 1 mm the proton flux increase due to focusing by the micro-lens was so strong that saturation of the film occurred. Quantitative data could only be obtained when the cylinder was moved to 5 mm from the proton foil, in order to collect a smaller part of the diverging proton beam. Under these conditions a small spot (less than 200 μm diameter was recorded on the detector (placed at several cm from the source), providing strong evidence of beam focusing and proton flux concentration. Due to the transient nature of the fields, the focusing was energy selective, as only protons passing through the cylinder while the fields were active were focused. Out of the broad proton beam spectrum, these are protons with energy such that the source-to-cylinder time of flight matches the time of arrival of the pulse irradiating the cylinder. Further investigations are planned to test the applicability of this method, and to understand the exact dynamics of the charged sheath and associated field at the inner surface of the cylinder. However the preliminary, proof-of-principle tests indicate that this is an extremely promising approach for focusing an intense proton beam, while at the same time selecting a desired energy range. The range can be tuned by varying parameters such as the relative delay of the laser pulses, and the relative distance of the targets employed. This technique could of interest for many of the proposed applications of laser-driven proton beams, e.g. isochoric heating for production of warm dense matter [19], proton-induced fast ignition [20], industrial and medical[21] applications, and for application as an ultrafast focusing/switching device for ion beams from conventional accelerators.

CONCLUSIONS

We have discussed here results pertaining to the detection and possible use of electric and magnetic transient fields initiated by high-intensity laser-interaction with matter. The use of laser-driven proton probes as a diagnostic tool has proven crucial in obtaining time and space resolve information on the structure and development of these fields, and consequently on the charge dynamics following high intensity laser-plasma interaction with underdense plasmas and solid targets. By this technique, important, previously unavailable information on the ion acceleration process has also been obtained. Understanding how these fields develop permits to envisage applications where they are controlled and employed to modify the properties of particle beams. Preliminary results relating to the focusing of laser-accelerated proton beams by using a laser-driven micro-lens appear extremely promising for obtaining

Downloaded 27 Aug 2012 to 146.48.102.127. Redistribution subject to AIP license or copyright; see http://proceedings.aip.org/about/rights_permissions

the enhanced flux concentration and narrow energy band required by many proposed applications.

ACKNOWLEDGMENTS

The authors acknowledge the support of the EU programme HPRI CT 1999-0052, of Grant No. E1127 from Region Ile-de-France, UNR grant DE-FC52-01NV14050, of Royal Society study visit grants, of DAAD, of British Council-MURST-CRUI, COST and INTAS Networks , of the SFB/TR18 programme and of the QUB/IRCEP scheme. Part of the PIC simulations were performed on the Linux cluster at the CINECA facility (Bologna, Italy), with the support of the INFM super-computing initiative. The authors acknowledge F. Cornolti, F. Pegoraro, S.V. Bulanov, M. Cuneo, T. Lysseikina and A. Pukhov for useful discussions, and the precious assistance of the laser and target area staff at LULI and RAL-CLF.

REFERENCES

1. E.L.Clark, *et al*., Phys. Rev. Lett. **84**, 670-673 (2000).
2. R.Snavely *et al*, Phys. Rev. Lett. **85**, 2945-2948 (2000).
3. M. Borghesi, *et al.*, Phys. Rev. Lett., **81**, 112-115 (1998).
4. K.Krushelnick *et al*, Phys. Rev. Lett., **83**, 737-740 (1999).
5. M. Borghesi, *et al.*, Phys Plasmas **9**, 2214-2220 (2002).
6. A.J. Mackinnon *et al.*, Rev. Sci. Instrum. **75**, 3531-3537 (2004).
7. T. Cowan, *et al.*, Phys. Rev. Lett. **92**, 204801 (2004).
8. M. Borghesi, *et al*., Phys. Rev. Lett. **92**, 055003 (2004).
9. M. Borghesi, *et al.*, Appl. Phys. Lett. **82**, 1529-1531 (2003).
10. M. Borghesi *et al.*, Phys. Rev. Lett. **88**, 135002 (2002).
11. M. Borghesi, *et al*., Phys. Rev. Lett. **94**, 145003 (2005).
12. S. P. Hatchett *et al.*, Phys. Plasmas **7**, 2076-2082 (2000).
13. S. Wilks *et al.*, Phys. Plasmas **8**, 542-549 (2001).
14. P. Mora, Phys. Rev. Lett. **90**, 185002 (2003).
15. L.Romagnani *et al*, Physical Review Letters, in press (2005).
16. M. Key *et al.*, Phys. Plasmas **5**, 1966-1972 (1998).
17. M. Passoni *et al.*, Laser and Particle Beams **22**, 163-168 (2004).
18. H. Ruhl *et al.*, Plasma Phys. Rep. **27**, 363-369 (2001).
19. P. Patel *et al.*, Phys. Rev. Lett. **91**, 125004 (2003).
20. M. Roth *et al.*, Phys. Rev. Lett. **86**, 436-439 (2001).
21. S.V. Bulanov *et al*., Phys. Lett. A **299**, 240-247 (2002).

Downloaded 27 Aug 2012 to 146.48.102.127. Redistribution subject to AIP license or copyright; see http://proceedings.aip.org/about/rights_permissions